Fast autofocus algorithm for automated microscopes

Mario A. Bueno-Ibarra
CITEDI-IPN
2498 Roll Drive 757
Otay Mesa, San Diego, California
and
CICESE
Dirección de Telemática
Km. 107 Carretera Tijuana-Ensenada
Ensenada, B.C. México, CP 22860
E-mail: mbueno@cicese.mx

Josué Álvarez-Borrego
CICESE
Dirección de Telemática
Km. 107 Carretera Tijuana-Ensenada
Ensenada, B.C. México, CP 22860

Leonardo Acho
CITEDI-IPN
2498 Roll Drive 757
Otay Mesa, San Diego, California

María Cristína Chávez-Sánchez
Centro de Investigación en Alimentación y Desarrollo, A. C.
Unidad Mazatlán en Acuicultura y Manejo Ambiental
Sábalo Cerritos S/N
Apdo. Postal 711
Estero del Yugo
Mazatlán Sinaloa, C.P. 82010, México

Abstract. We present a new algorithm to determine, quickly and accurately, the best-in-focus image of biological particles. The algorithm is based on a one-dimensional Fourier transform and on the Pearson correlation for automated microscopes along the *Z* axis. We captured a set of several images at different *Z* distances from a biological sample. The algorithm uses the Fourier transform to obtain and extract the image frequency content of a vector pattern previously specified to be sought in each captured image; comparing these frequency vectors with the frequency vector of a reference image (usually the first image that we capture or the most out-of-focus image), we find the best-in-focus image via the Pearson correlation. Numerical experimental results show the algorithm has a fast response for finding the best-in-focus image among the captured images, compared with related autofocus techniques presented in the past. The algorithm can be implemented in real-time systems with fast response, accuracy, and robustness; it can be used to get focused images in bright and dark fields; and it offers the prospect of being extended to include fusion techniques to construct multifocus final images.
[DOI: 10.1117/1.1925119]

Subject terms: automated microscope; focus algorithms; autofocusing; variance analysis; gradient filters; Fourier transform; Pearson correlation.

Paper 040582 received Aug. 25, 2004; accepted for publication Dec. 12, 2004; published online Jun. 20, 2005.

1 Introduction

Every day researchers in biological areas analyze a large number of microbiological samples. The need for fast, powerful, and reliable automated systems increases as these analyses deal with higher-resolution images. Some such developments have been described in the literature, e.g., an automatic system for identifying phytoplanktonic algae.[1] One step in an automatic system to capture microbiological images is to obtain the best-in-focus image from a biological sample. This is a challenging task.

Many autofocusing methods have been developed.[2–8] These methods use different approaches to obtain the best-in-focus image from a set of captured microscopic images. Among the algorithms developed for this purpose are the analysis of the global and local variance of the images' gray levels to get a measure of their contrast,[1,2] the use of first- and second-derivative operators to obtain a measure of the relative sharpness of images,[2,7,9–12,15] the analysis of gradient variance,[13] and the analysis of spatial frequency spectra.[14–16] All these algorithms have proven to be effective in obtaining the best-in-focus image; however, they require considerable time when the images have high resolution.

In the next sections we describe every algorithm involved in our computer experimentation. Section 2 provides a mathematical review of autofocus algorithm development based on global and local variance analysis or on image contrast. Section 3 describes autofocus algorithms based on first- and second-derivative operators to implement the image sharpness approach. Section 4 describes algorithms based on gradient variance analysis using the derivative operators described in Sec. 3. Section 5 introduces our new autofocus algorithm based on the analysis of spatial frequency spectra and exploiting the Fourier transform and Pearson correlation. Section 6 describes the computational experiments and provides the graphical results of those experiments, where we illustrate the performance of proposed algorithm compared with algorithms described in Secs. 2 to 4. And finally, Sec. 7 summarizes our conclusions and planned future work.

2 Autofocus Algorithm Based on Global Variance (GBL VAR)

Let us introduce some useful notation, definitions, and functions: $f_1, f_2, f_3, \ldots, f_K$ is a stack of K captured images of size $N \times M$ pixels from biological samples taken by stepping of the microscope in the Z direction in increments Δz;

0091-3286/2005/$22.00 © 2005 SPIE

$f(x,y)_k$ is the captured image matrix with pixels (x,y) in the k'th image in the stack, where $x=1,...,N$, $y=1,...,M$, and $k=1,...,K$.

Let $\hat{\mathbf{H}} \in \Re^{\Lambda}$ be a vector of real numbers with Λ elements sorted in ascending order. The maximum function $\mathrm{MAX}(\hat{\mathbf{H}})$ and minimum function $\mathrm{MIN}(\hat{\mathbf{H}})$ can be defined respectively as

$$\mathrm{MAX}(\hat{\mathbf{H}}) = \{h_{\Lambda} | h_i \leqslant h_{i+1}, \ \ h_i \in \hat{\mathbf{H}}, \ \ i=1,2,...,\Lambda-1\}, \tag{1}$$

$$\mathrm{MIN}(\hat{\mathbf{H}}) = \{h_1 | h_i \leqslant h_{i+1}, \ \ h_i \in \hat{\mathbf{H}}, \ \ i=1,2,...,\Lambda-1\}. \tag{2}$$

The normalized transformation function $N(\hat{\mathbf{H}})$ can be expressed as

$$N(\hat{\mathbf{H}}) = \left\{ \frac{h_i - \mathrm{MIN}(\hat{\mathbf{H}})}{\mathrm{MAX}(\hat{\mathbf{H}}) - \mathrm{MIN}(\hat{\mathbf{H}})} \middle| h_i \in \hat{\mathbf{H}}, i=1,2,...,\Lambda \right\}, \tag{3}$$

where $N(\hat{\mathbf{H}}) \rightarrow [0,1]$ results in a vector of normalized values. The greatest-integer function $\lfloor \omega \rfloor$ of a number can be expressed as

$$\lfloor \omega \rfloor = \{\delta | \delta \in Z, \ \ \omega \in \Re, \ \ \delta \leqslant \omega < \delta + 1\}, \tag{4}$$

where Z represent the set of whole numbers.

In this approach, the best-in-focus image can be expected to have a strong variation in pixel intensity level;[1,2] the image with highest contrast will be the best-in-focus image in the stack. In this context, if we calculate the global variance GV_k of each f_k, then GV_k can be used to construct a focus measure, such that the best-in-focus image f_{BF} will have the maximum calculated value of GV_k:

$$f_{\mathrm{BF}} = \{f_k \ \ \text{where} \ \ \mathrm{MAX}(N(\mathrm{GVFM}_k)), \tag{5}$$

where GVFM_k is a vector of GV_k values, calculated for each f_k. Here GVFM_k can be obtained by calculating the local variance $\mathrm{LV}(n,m)_k$ of a moving window of size $\omega_x \times \omega_y$ for each pixel $f(n,m)_k$. Therefore, $\omega_x = \{2\xi_1 + 1 | \xi_1 \in \mathrm{Z}^+, 2\xi_1 + 1 \leqslant N\}$ and $\omega_y = \{2\xi_2 + 1 | \xi_2 \in \mathrm{Z}^+, 2\xi_2 + 1 \leqslant M\}$, where $Z^+ = \{\tau | \tau \in Z, \tau > 0\}$ and ξ_1, ξ_2 are the dimensions of the moving window. The variance $\mathrm{LV}(n,m)_k$ can be computed for each displacement of the moving window across image $f(n,m)_k$:

$$\mathrm{LV}(n,m)_k = \frac{1}{\omega_x \omega_y - 1} \sum_{i=\omega x_1}^{\omega x_2} \sum_{j=\omega y_1}^{\omega y_2} [f(i,j)_k - \overline{\mathrm{LV}(n,m)_k}]^2, \tag{6}$$

where $\overline{\mathrm{LV}(n,m)_k}$ is the mean value of the pixel intensity in the moving window centered on (n,m), given by

$$\overline{\mathrm{LV}(n,m)_k} = \frac{1}{\omega_x \omega_y} \sum_{i=\omega x_1}^{\omega x_2} \sum_{j=\omega y_1}^{\omega y_2} f(i,j)_k, \tag{7}$$

and where ωx_1, ωx_2, ωy_1, ωy_2 are values to delimit the pixels of the moving window to be processed by Eq. (6) and Eq. (7). Let us define $\beta_1 = \lfloor \omega_x/2 \rfloor$, $\beta_2 = \lfloor \omega_y/2 \rfloor$. Then ωx_1, ωx_2, ωy_1, ωy_2 can be expressed as

$$\begin{aligned} \omega x_1 &= n - \beta_1, \quad \omega y_1 = m - \beta_2, \\ \omega x_2 &= n + \beta_1, \quad \omega y_2 = m + \beta_2, \end{aligned} \tag{8}$$

and the moving window is processed for each pixel (n,m) inside $f(n,m)_k$. Therefore n and m can be listed across $f(n,m)_k$ as

$$n \in \{\beta_1 + 1, \beta_1 + 2, ..., N - (\beta_1 + 1), \ N - \beta_1\}, \tag{9}$$

$$m \in \{\beta_2 + 1, \beta_2 + 2, ..., M - (\beta_2 + 1), \ M - \beta_2\}. \tag{10}$$

The global variance focus measure vector GVFM_k can be expressed as

$$\mathrm{GVFM}_k = \frac{1}{\alpha_1 \alpha_2 - 1} \sum_{p=n_I}^{n_F} \sum_{q=m_I}^{m_F} [\mathrm{LV}(p,q)_k - \overline{\mathrm{LV}_k}]^2, \tag{11}$$

where $\alpha_1 \alpha_2$ is the number of moving windows processed inside $f(n,m)_k$, and α_1, α_2 are defined by

$$\alpha_1 = N - 2\beta_1, \quad \alpha_2 = M - 2\beta_2. \tag{12}$$

From Eq. (9) and Eq. (10) we can obtain

$$\begin{aligned} n_I &= \beta_1 + 1, \quad n_F = N - \beta_1, \\ m_I &= \beta_2 + 1, \quad m_F = M - \beta_2, \end{aligned} \tag{13}$$

and $\overline{\mathrm{LV}}_k$, the mean value of all local variances of the moving windows processed inside the image $f(n,m)_k$, can be expressed by

$$\overline{\mathrm{LV}}_k = \frac{1}{\alpha_1 \alpha_2} \sum_{p=n_I}^{n_F} \sum_{q=m_I}^{m_F} \mathrm{LV}(p,q)_k. \tag{14}$$

3 Autofocus Algorithms Based on Differentiation

These methods are based on the use of first and second derivatives. The objective of this approach is to find the image with the sharpest edges; hence image gradients are applied for calculating the focus measure.[2,15]

3.1 *Tenenbaum's Algorithm (SOB-TEN)*

This algorithm belongs to the first-derivative methods. In 1970, Tenenbaum developed a focus measure method based on obtaining the gradient magnitude from the Sobel operator.[9] The resulting algorithm was called the Tenengrad method, and it was considered the benchmark in this field.[7,10] The best-focused image f_{BF} in the stack can be obtained for the expression

$$f_{\mathrm{BF}} = \{f_k \ \ \text{where} \ \ \mathrm{MAX}(N(\mathrm{STFM}_k)), \tag{15}$$

where STFM_k is a vector of normalized maximum magnitudes calculated by the Tenengrad method for f_k:

$$\mathrm{STFM}_k = \sum_{n=2}^{N-1} \sum_{m=2}^{M-1} [\nabla S(n,m)_k]^2 \quad \text{for } \nabla S(n,m)_k > T, \tag{16}$$

where T is a discrimination threshold value, and $\nabla S(n,m)_k$ is the Sobel gradient magnitude value expressed by

$$\nabla S(n,m)_k = [\nabla S_x(n,m)_k^2 + \nabla S_y(n,m)_k^2]^{1/2}, \tag{17}$$

where $\nabla S_x(n,m)_k$, $\nabla S_y(n,m)_k$ are the outcome values obtained from the Sobel convolution masks S_x, S_y, respectively, defined by

$$S_x = \begin{pmatrix} -1 & 0 & 1 \\ -2 & 0 & 2 \\ -1 & 0 & 1 \end{pmatrix}, \quad S_y = \begin{pmatrix} 1 & 2 & 1 \\ 0 & 0 & 0 \\ -1 & -2 & -1 \end{pmatrix}. \tag{18}$$

Thus, $\nabla S_x(n,m)_k$, $\nabla S_y(n,m)_k$ can be expressed by

$$\begin{aligned} \nabla S_x(n,m)_k = \{ & -[f(n-1,m-1) + 2f(n-1,m) \\ & + f(n-1,m+1)] + [f(n+1,m-1) \\ & + 2f(n+1,m) + f(n+1,m+1)]\}_k, \\ \nabla S_y(n,m)_k = \{ & +[f(n-1,m-1) + 2f(n,m-1) \\ & + f(n+1,m-1)] - [f(n-1,m+1) \\ & + 2f(n,m+1) + f(n+1,m+1)]\}_k. \end{aligned} \tag{19}$$

3.2 *Boddeke's Algorithm (BOD)*

This algorithm also belongs to the first-derivative methods. In 1994, Boddeke proposed a new focus-measure algorithm based on calculating a gradient magnitude value using a one-dimensional convolution mask along the x image direction only. The convolution mask was defined by $B_x = [-1\ 0\ 1]$.[11] This method is considered extremely simple and provides a sharp, well-formed peak.[12] Therefore, the best-in-focus image f_{BF} in the stack can be obtained as

$$f_{\mathrm{BF}} = \{f_k \text{ where } \mathrm{MAX}(N(\mathrm{BFM}_k)), \tag{20}$$

where BFM_k is a vector with normalized values. After using Boddeke's convolution mask B_x on f_k, BFM_k can be expressed as

$$\mathrm{BFM}_k = \sum_{n=2}^{N-1} \sum_{m=1}^{M} [\nabla B_x(n,m)_k]^2, \tag{21}$$

where $\nabla B_x(n,m)_k$ is a value obtained by applying B_x to the pixel location (n,m) in the image:

$$\nabla B_x(n,m)_k = f(n+1,m) - f(n-1,m). \tag{22}$$

3.3 *Second-Derivative Algorithm (LAP)*

Another methodology for analyzing high spatial frequencies associated with image border sharpness is the application of the second-derivative methods. The simplest second-derivative operator, as shown by Rosenfeld and Kak in 1982, is the Laplacian operator.[15] By applying this operator to each image f_k in the stack, one can find the best-in-focus image f_{BF}:

$$f_{\mathrm{BF}} = \{f_k \text{ where } \mathrm{MAX}(N(LFM_k)), \tag{23}$$

where LFM_k is a vector with normalized values found by applying the Laplacian operator L with convolution mask, defined by

$$L = \frac{1}{6} \begin{pmatrix} 0 & -1 & 0 \\ -1 & 4 & -1 \\ 0 & -1 & 0 \end{pmatrix}. \tag{24}$$

Thus, LFM_k can be expressed as

$$\mathrm{LFM}_k = \sum_{n=2}^{N-1} \sum_{m=2}^{M-1} |\nabla L(n,m)_k|, \tag{25}$$

where $|\nabla L(n,m)_k|$ is an absolute value of the Laplacian gradient defined by

$$\begin{aligned} \nabla L(n,m)_k = \frac{1}{6}\{ & 4f(n,m) - [f(n-1,m) + f(n,m-1) \\ & + f(n+1,m) + f(n,m+1)]\}. \end{aligned} \tag{26}$$

4 Autofocus Algorithms Based on the Gradient Variance

A complementary strategy is to calculate a gradient magnitude variance, such as the Sobel-Tenengrad or the Laplacian magnitude gradient variance. This methodology defines a highly discriminating focus measure, increasing the robustness to noise.[13]

4.1 *Sobel-Tenengrad Gradient Magnitude Variance (SOB VAR)*

This new strategy was proposed by Pech-Pacheco and Cristóbal.[13] The best-in-focus image f_{BF} in the stack based on the Sobel-Tenengrad gradient magnitude variance will be the image with highest variance in the sense

$$f_{\mathrm{BF}} = \{f_k \text{ where } \mathrm{MAX}(N(\mathrm{STVFM}_k)), \tag{27}$$

where STVFM_k is a vector containing normalized values. After applying the Sobel-Tenengrad gradient algorithm and calculating its variance, defined in Sec. 3.1, STVFM_k can be expressed as

$$\begin{aligned} \mathrm{STVFM}_k = & \sum_{n=2}^{N-1} \sum_{m=2}^{M-1} [\nabla S(n,m)_k - \overline{\nabla S(n,m)_k}]^2 \\ & \text{for } \nabla S(n,m)_k > T, \end{aligned} \tag{28}$$

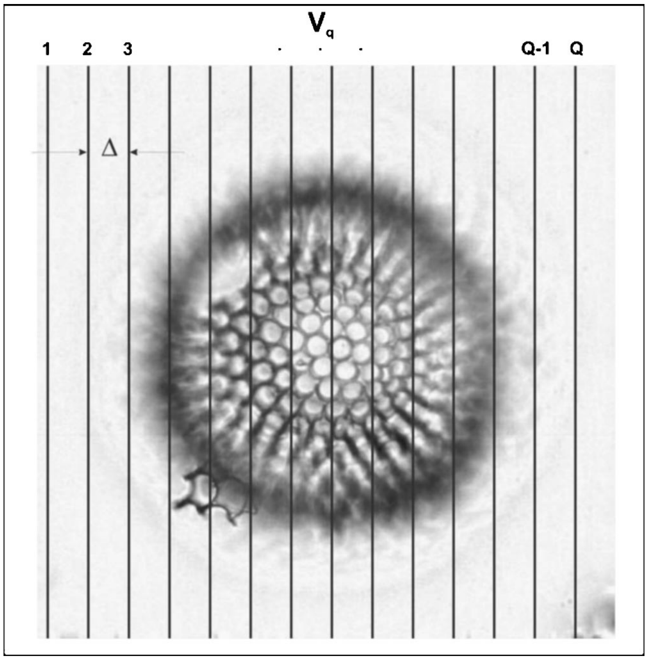

Fig. 1 Scan process pattern defined by vectors V_q across one sample captured image.

where T is a discrimination threshold value, $\nabla S(n,m)_k$ is the Sobel-Tenengrad gradient magnitude value expressed by Eq. (17), and $\overline{\nabla S(n,m)_k}$ is the Sobel-Tenengrad gradient magnitude mean value, defined by

$$\overline{\nabla S(n,m)_k}=\frac{1}{(N-2)(M-2)}\sum_{n=2}^{N-1}\sum_{m=2}^{M-1}\nabla S(n,m)_k. \tag{29}$$

4.2 *Laplacian Gradient Magnitude Variance (LAP VAR)*

Continuing with these approaches, the best-in-focus image f_{BF} in the stack, according to the Laplacian gradient magnitude variance, will be the image with highest variance,[13] in this context

$$f_{\mathrm{BF}}=\{f_k \text{ where } \mathrm{MAX}(N(\mathrm{LPVFM}_k)), \tag{30}$$

where LPVFM_k is a vector containing normalized values. After applying the Laplacian gradient algorithm and calculating its variance, defined in Section 3.3, LPVFM_k can be expressed as

$$\mathrm{LPVFM}_k=\sum_{n=2}^{N-1}\sum_{m=2}^{M-1}[\nabla L(n,m)_k-\overline{\nabla L(n,m)_k}]^2, \tag{31}$$

where $\nabla L(n,m)_k$ is the Laplacian gradient magnitude value expressed by Eq. (26), and $\overline{\nabla L(n,m)_k}$ is Laplacian magnitude mean value, defined by

$$\overline{\nabla L(n,m)_k}=\frac{1}{(N-2)(M-2)}\sum_{n=2}^{N-1}\sum_{m=2}^{M-1}\nabla L(n,m)_k. \tag{32}$$

5 New Autofocus Algorithm Based on One-Dimensional Fourier Transform and Pearson Correlation (P.CORR)

We propose here a new, fast algorithm to get the best-in-focus image f_{BF}, based on use of the Fourier transform to obtain the spatial frequency content of each captured image in the stack, and the Pearson correlation to construct a normalized focus measure. When we work with digital images captured by CCD, these images are functions on the spatial domain, so that we will work in the spatial domain instead

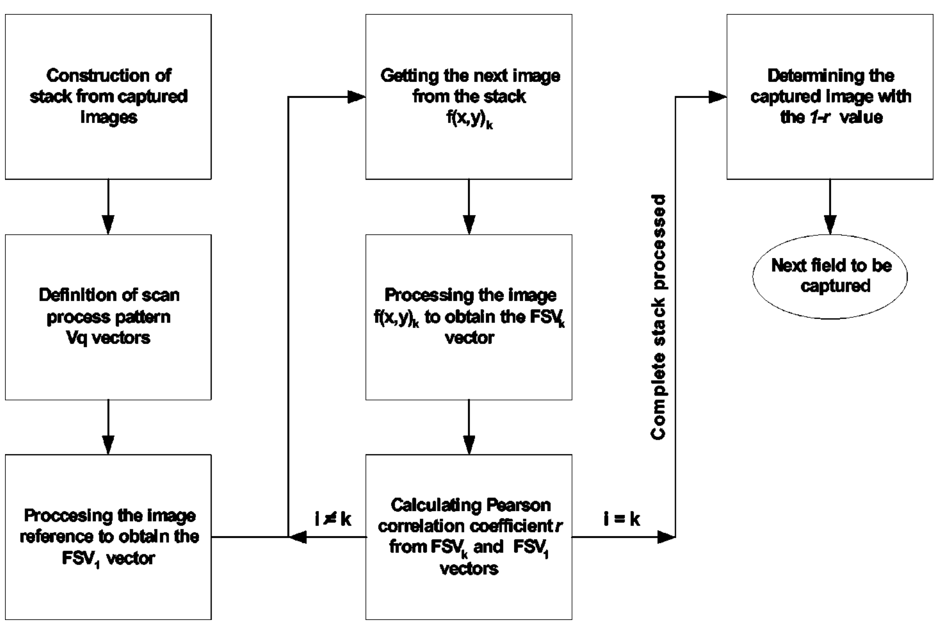

Fig. 2 General proposed algorithm diagram.

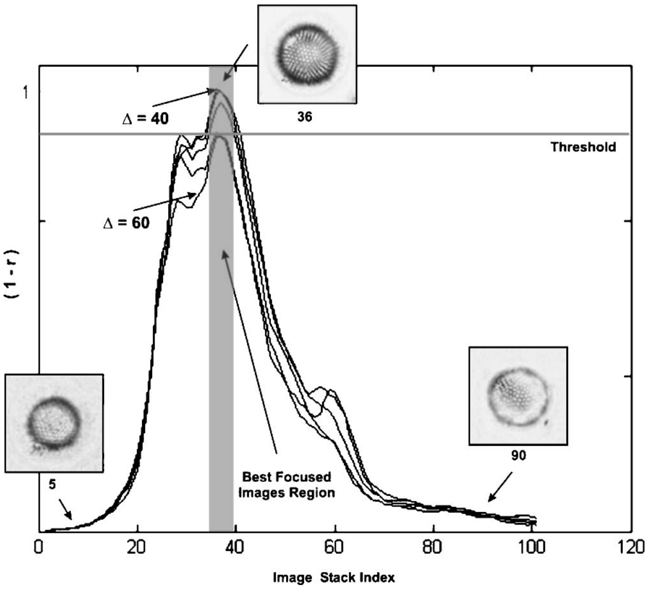

Fig. 3 Bright-field curves of $1-r$ with $\Delta=40$ to 60 pixels, showing the best-in-focus image and its index from the captured image stack.

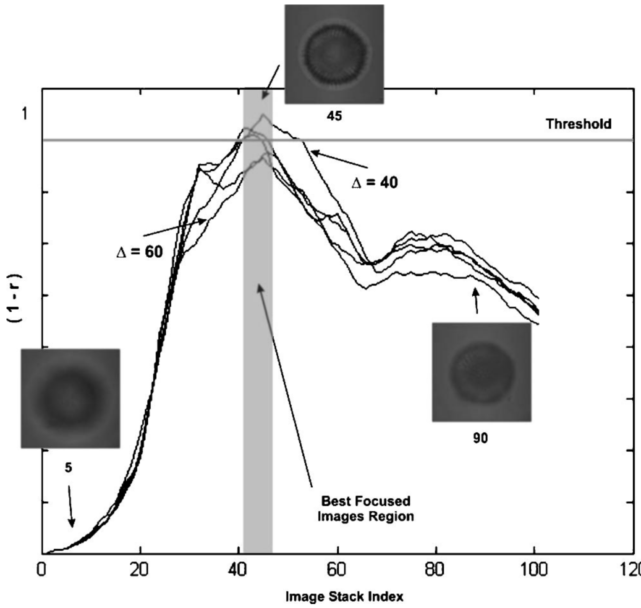

Fig. 5 Dark-field curves of $1-r$ with $\Delta=40$ to 60 pixels, showing the best-in-focus image and its index from the captured image stack.

of the time domain. Let us review some useful definitions: The spatial-frequency one-dimensional Fourier transform integral pair can be defined by the expressions

$$H(f)=\int_{-\infty}^{\infty} h(x)\exp(-j2\pi f x)\mathrm{d}x \tag{33}$$

and

$$h(x)=\int_{-\infty}^{\infty} H(f)\exp(j2\pi f x)\mathrm{d}f. \tag{34}$$

Thus, in Eq. (33), $H(f)$ is the spatial one-dimensional Fourier transform of $h(x)$, and in Eq. (34), $h(x)$ is the spatial one-dimensional inverse Fourier transform of $H(f)$. Typically, $h(x)$ is termed a function of the space variable and $H(f)$ is termed a function of the spatial frequency variable.

The linear correlation coefficient is r sometimes referred to as the simple correlation coefficient, the Pearson product moment correlation coefficient, or just the Pearson correlation. It is a measure of intensity of association between two variables X and Y,[17] and can be obtained from the expression

$$r=\frac{\sum XY-\dfrac{\sum X\sum Y}{\eta}}{\left\{\left[\sum X^2-\dfrac{(\sum X)^2}{\eta}\right]\left[\sum Y^2-\dfrac{(\sum Y)^2}{\eta}\right]\right\}^{1/2}}, \tag{35}$$

where η represents the number of pairs of data present.

The Pearson coefficient r can never be greater than 1.0 nor less than -1.0; therefore we use $|r|$ to measure the intensity of association (correlation) between the two variables X and Y. Obtaining a value of r close to 0.0 means that no correlation exists between the variables; obtaining a value close to 1.0 means that a strong correlation exists between them.

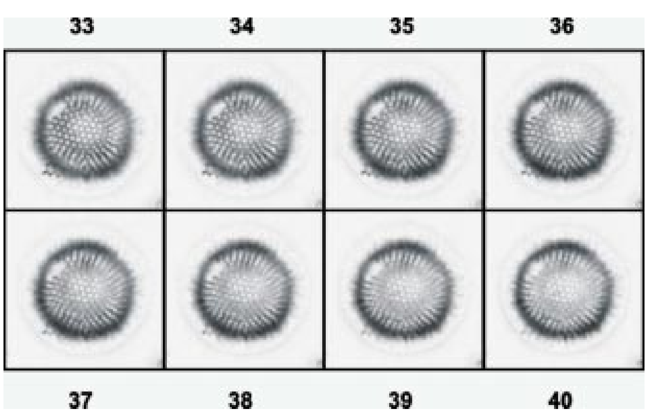

Fig. 4 Bright-field images with similar Pearson coefficient values $1-r$.

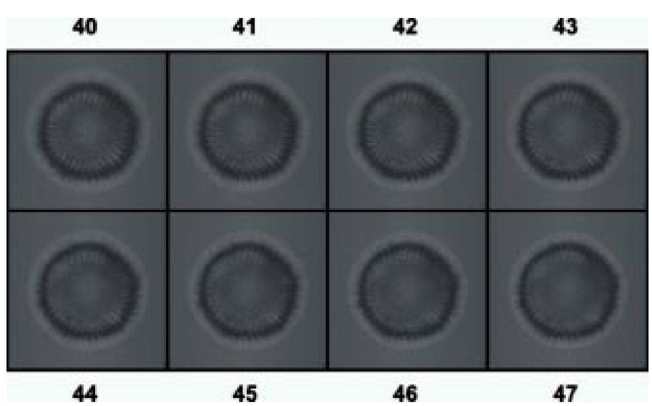

Fig. 6 Dark-field images with similar Pearson coefficient values $1-r$.

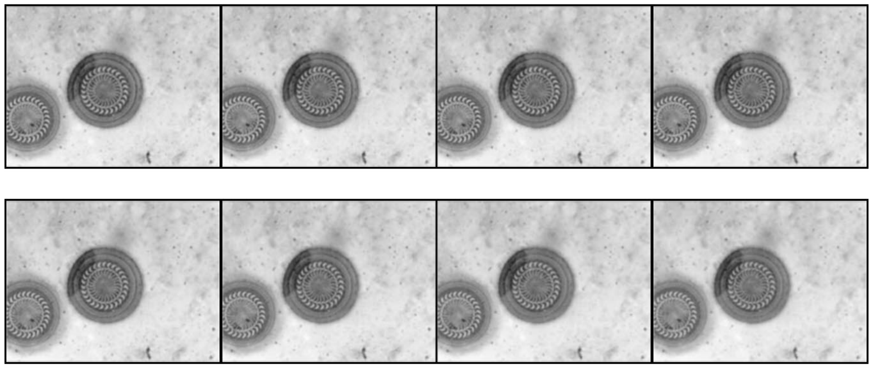

Fig. 7 Images inside the best-focus region obtained from the tested algorithms.

5.1 *Fourier Transform and Pearson Correlation Algorithm*

Once we have built a stack of captured images, the proposed algorithm processes a group of Q vectors V_q, $q = 1,...,Q$, which are spatially equidistant. They constitute a scan process pattern corresponding to each captured image $f(x,y)_k$. In Fig. 1, Δ denotes the distance between adjacent vectors. Thus the algorithm does not process the entire image, only the pattern defined. The number of vectors, Q, can be calculated as $Q = \lfloor N/\Delta \rfloor + 1$, where $\lfloor N/\Delta \rfloor$ is, according to Eq. (4), a whole number. The vectors V_q can be computed by

$$V_1 = f(1, y_0, \ldots, y_M)_k,$$
$$V_2 = f(1+\Delta, y_0, \ldots, y_M)_k, \ldots, \tag{36}$$
$$V_q = f((q-1)\Delta + 1, y_0, \ldots, y_M)_k.$$

Computing the Fourier power spectrum of the V_q, we get $|H_1(f)|^2$, $|H_2(f)|^2, \ldots, |H_q(f)|^2$, respectively. With these Fourier spectrum vectors, containing the high and low frequencies of the vectors V_q, we build a unique concatenated Fourier power spectrum vector FSV_k for the captured image $f(x,y)_k$. We compute FSV_k from each captured image and compare them by Pearson correlation with FSV_1 for the first captured image $f_1(x,y)$, which is called the image reference and chosen to be the most out-of-focus image. Thus we obtain f_{BF} that minimizes the Pearson correlation coefficient r. The most out-of-focus image will have a lower correlation value than f_{BF}. In this context, f_{BF} can be obtained as

$$f_{\mathrm{BF}} = \{ f_k \ \text{ where } \ \mathrm{MIN}(N(r_k)), \tag{37}$$

where r_k is a vector containing normalized values of the correlation r.

In Eq. (35) we take $X = \mathrm{FSV}_1$ and $Y = \mathrm{FSV}_k$ for each computation of the Pearson coefficient r, and η as the length of the vectors X and Y. Figure 1 shows the scan process pattern defined by vectors V_q according to Eq. (36). We can control the spacing of the V_q by changing the value of variable Δ. Letting $\Delta \to 1$, we will have more vectors to compute; letting $\Delta \to N$, we will have fewer, and the algorithm will be less sensitive to details of the sample. In the experiments we use different Δ values and obtain graphs of the corresponding algorithm sensitivities for use in deciding on the final focused image. Finally, Fig. 2 shows a general diagram of the algorithm proposed.

Table 1 Execution-time performance results and f_{BF} image indices obtained.

	Res. 522×387		1044×775		1566×1162		2088×1550	
Algorithm	Best-in-focus image	Execution time (s)	Best-in-focus image	Execution time (s)	Best-in-focus image	Execution time (s)	Best-in-focus image	Execution time (s)
GBL VAR	30	1603	31	6762	31	15513	32	27703
SOB TEN	32	365	34	1474	34	3354	34	5997
BOD	33	72	34	282	34	659	34	1181
LAP	41	130	41	509	41	1174	44	2103
SOB VAR	33	374	41	1461	34	3303	34	5843
LAP VAR	34	150	34	560	35	1281	34	2311
P.CORR (this study)	29	5	30	13	30	52	30	111

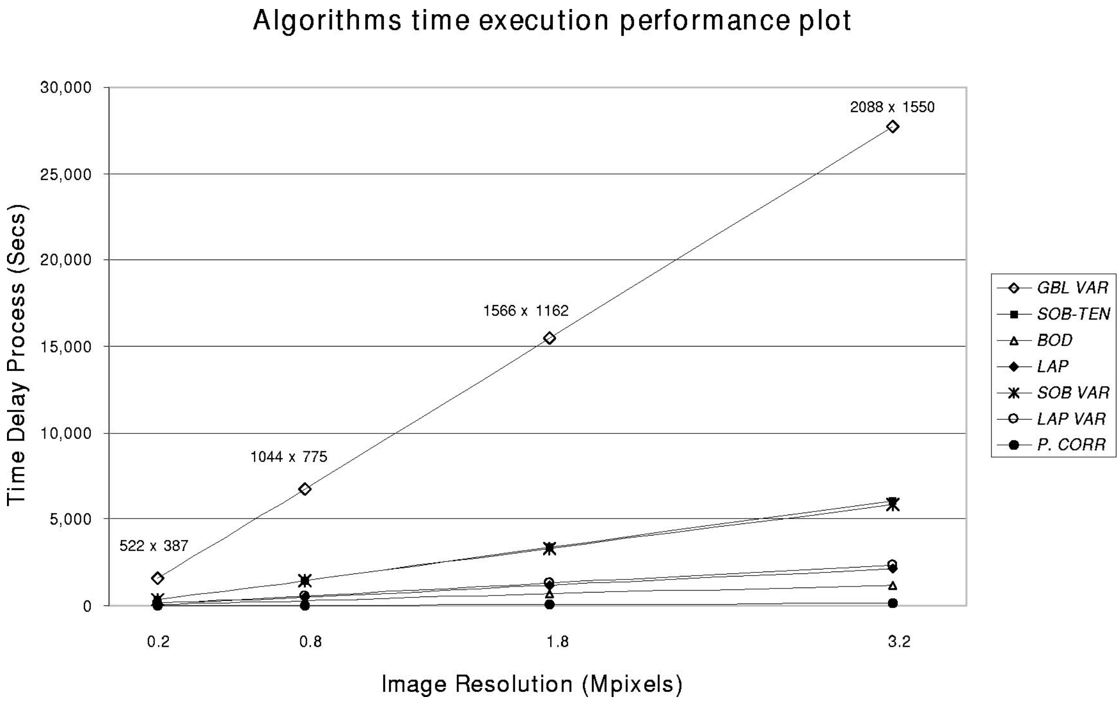

Fig. 8 Graphs of execution time for the tested algorithms.

6 Computational Experiments

Two kinds of computer experiments were developed. The first kind were related to getting f_{BF} with the proposed algorithm. To test the algorithm, independent images of biological samples were used for measurement of computational process times; namely dark- and bright-field images were captured from the same biological organism. The second kind of experiments were to measure the computational process times of every algorithm described in the preceding section. For these, an entirely new set of biological images were captured.

6.1 *Experiments Related to Getting f_{BF} from the Proposed Algorithm*

Generally, when we are manually focusing on a sample under a microscope, several images close to the focus point can be suitable candidates for the best focus. Our choice will depend on external factors, such as our vision, the microscope lenses, the illumination, and the sample itself; but at last we select one as best. The method proposed operates in the same way that we do: it decides what is the best image to display, by checking the Pearson coefficient r.

Figure 3 shows the curves of $1-r$ when we change the Δ value in the range 40 to 60 pixels with increments of 5 pixels. It is important to mention that $\Delta=60$ means that just nine vectors V_q were processed. We observe that all peaks of the graphs are inside the best-in-focus image region. When $\Delta \to N$ the algorithm runs faster but we lose sensitivity, so that we cannot find the best-in-focus image. The graphics from the experiments show that 36th image index has the best decorrelation value.

The difference between the images shown in the best-focus region (Fig. 4) is not noticeable. These images are all inside the region where we seek the best-in-focus image.

Figures 5 and 6 show similar results to those we obtained before. The main difference is that we work with dark-field images. We observe that the algorithm can find the best-in-focus image with the same values of the variables. In this situation, we can declare that this algorithm works automatically in both types of fields without any change. To determine the best-focus region, we propose to include all images with normalized focus measure $1-r_k$ greater than a threshold T_{BFR}. The images f_k selected from the stack to be inside the focusing region can be determined by the heuristic discrimination rule $1-r_k \geqslant T_{BFR}$, namely, $1-r_k \geqslant 0.95$.

6.2 *Experiments Related to Measuring the Computational Process Times of Algorithms*

To measure the proposed algorithm's performance and compare it with that of the algorithms cited in Sec. 5, we captured four stacks with 60 images per stack of a new biological sample, where every image in the stack was taken at different pixel resolution: 522×387, 1044×775, 1566×1162, and 2088×1550. Thus, we have images with sizes of 0.2, 0.8, 1.8, and 3.2 megapixels, respectively.

The moving-window size used in the global variance algorithm was 25×25 pixels to increase the algorithm sensitivity. In this case, the control moving-window size variables ξ_1, ξ_2 were both initialized at 12. Finally, the spacing Δ of the vectors V_q in our proposed algorithm was initialized at 35 pixels to be compatible with the moving-window size in the global variance algorithm. No more initialized variables were needed to get the final results. The equipment used for the tests was a 2.5-GHz PC Pentium 4 with 1-Gbyte RAM and 80-Gbyte hard disk.

Figure 7 shows the images inside the best-focus region obtained from the tested algorithms. Table 1 summarizes the execution-time performance results and the f_{BF} image index obtained from the algorithms tested. We can see clearly that the proposed algorithm has the best execution time and that the resulting f_{BF} is inside the best-focus region. One exception was the Laplacian algorithm, where f_{BF} was out of the best-focus region. However, when the Laplacian gradient magnitude variance algorithm was used, the f_{BF} found was inside the best-focus region. Finally, Fig. 8 shows graphs of the execution time, where we can see clearly that the proposed algorithm (P.CORR) is the fastest among the tested algorithms.

7 Conclusions and Future Work

The proposed focusing method offers significant improvements in accuracy, robustness, and speed, and is suitable for implementation in real-time processing; besides, it can process different types of environments with respect to illumination, bright or dark field, and image resolution. Further work will include incorporating fusion techniques in the proposed algorithm to improve the final image quality; this can be done by finding the optimum threshold value whereby we can combine the images inside the focusing region to construct a new, final high-quality image. For this purpose, studies are needed to design and test new scan process patterns and kernels, based on the Fourier transform, for incorporation in the proposed algorithm.

Acknowledgments

Part of this work was supported by the Mexican National Council of Science and Technology (CONACYT, project 36075-B). Thanks are due to María Amparo Rodríguez-Santiago for the samples shown in Fig. 7.

References

1. J. L. Pech-Pacheco, G. Cristóbal, J. Alvarez-Borrego, and L. Cohen, "Automatic system for phytoplanktonic algae identification," *Limnética* **20**(I), 143–158 (2001).
2. J. L. Pech-Pacheco, G. Cristóbal, I. Chamorro-Martínez, and J. Fernández-Valdivia, "Diatom autofocusing in lighting microscopy: a comparative study," in *Int. Conf. on Pattern Recognition*, pp. 318–321 (2000).
3. W. Bocker, W. Rolf, W. Muller, and C. Streffer, "Investigations about autofocus-algorithms for fluorescent-microscopy," in *Applications of Digital Image Processing XIX, Proc. SPIE* **2847**, 445–456 (1996).
4. M. Subbarao and A. Nikzad, "Focusing techniques," *Opt. Eng.* **32**(11), 2824–2836 (1993).
5. T. Yeo, S. Ong, L. Jayasooriah, and R. Sinniah, "Autofocusing for tissue microscopy," *Image Vis. Comput.* **11**(10), 629–639 (1993).
6. L. K. Firestone, K. Cook, K. Culp, N. Talsania, and K. Preston, "Comparisons of autofocus methods for automated microscopy," *Cytometry* **12**, 195–206 (1991).
7. E. Krotkov, "Focusing," *Int. J. Comput. Vis.* **I**, 223–237 (1987).
8. F. Groen, I. T. Young, and G. Ligthard, "A comparison of different focus functions for use in autofocus algorithms," *Cytometry* **6**, 81–91 (1985).
9. J. M. Tenenbaum, "Accommodation in computer vision," PhD Dissertation, Stanford Univ. (1970).
10. J. F. Schlag, A. C. Sanderson, C. P. Neuman, and F. C. Wimberly, "Implementation of automatic focusing algorithms for computer vision system camera control," Technical Report CMU-RI-TR-83-14, Robotics Institute, Carnegie Mellon Univ. (1983).
11. F. R. Boddeke, L. J. Van Vliet, H. Netten, and I. T. Young, "Autofocusing in microscopy based on the OTF and sampling," *Bioimaging* **2**, 193–203 (1994).
12. S. L. Ellenberger and I. T. Young, "Microscope image acquisition," in *Image Processing and Analysis*, R. Baldock and J. Graham, Eds., Oxford Univ. Press, Oxford (1998).
13. J. L. Pech-Pacheco and G. Cristóbal, "Diatom autofocusing in bright field microscopy: a comparative study," in *Proc. Int. Conf. on Pattern Recognition*, Vol. 3, pp. 318–321, IEEE Computer Soc., Los Alamitos, CA (2000).
14. E. O. Brigham, *The Fast Fourier Transform and Its Applications*, pp. 9–11, Prentice-Hall, Englewood Cliffs, NJ (1988).
15. R. González and R. Woods, *Digital Image Processing*, 2nd ed., pp. 125, 128–130, 151–152, Prentice-Hall (2002).
16. J. Russ, *The Image Processing Handbook*, CRC Press, Boca Raton, FL (1995).
17. J. H. Zar, *Biostatistical Analysis*, 3rd ed., pp. 371–373, Prentice-Hall (1996).

Mario A. Bueno-Ibarra received his MEng degree in automation and control at Universidad Autónoma de Ciudad Juárez in 1996 and is finishing his PhD in communication and electronics at CITEDI-IPN. His work is related to biological image processing topics.

Josué Álvarez-Borrego received his BS degree in physical oceanography in 1981 from the Facultad de Ciencias Marinas, Ensenada, B. C., México, and his MSc and PhD degrees in optics in 1983 and 1993 from CICESE, México. He is a titular researcher with the Telematic Directions, CICESE, México. His research interests are image processing with applications to biogenic particles and image processing of the sea surface. He is the author of several scientific papers and presentations at scientific conferences. He is a member of the Mexican Academy of Optics, Researches National System (SNI), and the Sciences Mexican Academy.

Leonardo Acho received the MSc degree in electronics systems at ITESM-Monterrey, Mexico, in 1992 and the PhD degree in automatic control from CICESE, Mexico, in 2001. Currently he is with the Digital Technology Research and Development Center (CITEDI-IPN), Mexico.

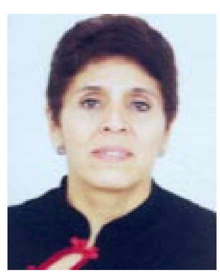

María Cristína Chávez-Sánchez received her biological degree in 1971, her MSc in 1983, and her PhD in aquaculture and fisheries management in 1987 from the Stirling University. Currently she is a researcher in the Mazatlan Unit on Aquaculture and Environmental Management of the Research Center of Feeding and Development (CIAD, A.C.). Her research interest is aquatic pathology.